Int. J. Heat Mass Transfer. Vol. 35, No. 1, pp. 141–153, 1992
Printed in Great Britain

0017–9310/92 $5.00 + 0.00

Numerical modelling of phase change and heat transfer during rapid solidification processes: use of control volume integrals with element subdivision

G.-X. WANG and E. F. MATTHYS

Department of Mechanical and Environmental Engineering, University of California, Santa Barbara, CA 93106, U.S.A.

(*Received* 23 *April* 1990 *and in final form* 3 *January* 1991)

Abstract An effective interface-tracking scheme has been developed for the numerical modelling of heat transfer and phase change during rapid solidification. This technique is based on Control Volume Integrals, and achieves high-resolution tracking of the solid/liquid interface by element subdivision. It is particularly well-suited for rapid solidification with undercooling, for which the accurate prediction of the interface temperature during recalescence is very important. This approach has been used to model the Planar Flow Casting and Splat Cooling processes. Some results on temperature profiles and on interface velocity, location, undercooling, and cooling rate are shown for both processes.

1. INTRODUCTION

MUCH WORK has been conducted in the past on the numerical modelling of phase change. Recently, however, the development of Rapid Solidification Processes (RSP) has posed new challenges because of the associated large cooling rates and undercooling which introduce additional difficulties in modelling. Strictly speaking, solidification always requires a certain degree of undercooling (although often very small), but this undercooling may become particularly large in RSP processes.

In the classic solidification case (the Stefan problem), the undercooling is small enough that it is reasonable to use an assumption of local thermodynamic equilibrium at the solid/liquid interface. The interface moves into the superheated liquid, and energy is conducted away through the solid. The interface velocity is controlled primarily in this case by the rate of external heat extraction. Such a situation is expressed mathematically by a fixed interface temperature condition (assumed to be the melting temperature determined by the material's phase diagram). On the other hand, large undercooling levels may exist during rapid solidification. In this case, the interface cannot be assumed to be in thermodynamical equilibrium, and kinetics effects must be taken into account. The interface temperature is then a function of time and of the process parameters. This variation in interface temperature introduces an extra degree of freedom which is constrained by a kinetics relationship between interface velocity and undercooling. The solidification rate is therefore controlled not only by the external heat extraction but also by crystal growth kinetics.

Exact analytical solutions to the Stefan problem are available only for very restrictive boundary conditions [1, 2], however, and several numerical techniques had to be developed for more general boundary conditions. Among the main finite difference techniques, the interface-tracking and enthalpy approaches are well known and address the question of the moving solid/liquid interface rather differently [3–6]. However, only a few studies have been conducted on solidification of crystalline materials with large undercooling. Shingu and Ozaki [7], for example, calculated the solidification rate during splat cooling based on an isothermal phase change model with a solidification temperature different from the equilibrium value. In this study, an approximate average undercooling is determined by matching the solidification rate calculated from the heat flow balance to the crystal growth rate calculated by a kinetics relationship. Levi and Mehrabian [8], investigated the rapid solidification of powders by incorporating the kinetics relationship within the heat transfer model itself and calculated the interface undercooling. They used the enthalpy method to generate the finite difference equations, but solved them directly for the temperature. Clyne [9] developed a finite difference model of rapid solidification that is based on a local heat source approach assuming a uniform latent heat release over the volume element containing the interface. This method has also been used by Chu *et al.* [10] to model planar flow casting.

A key parameter determining the microstructure of rapidly-solidified materials is the solid/liquid interface velocity [11], and a good model should predict accurately this velocity and the interface temperature. This is particularly critical during recalescence when the undercooling and the interface velocity are coupled.

NOMENCLATURE

a, b, c, d	coefficients in the difference equations
b	thickness of the sample
c_1, c_2	coefficients in the difference equations
c_P	specific heat
D	diameter of the wheel
E_V	activation energy
h	heat transfer coefficient
H	melt puddle height
ΔH_m	heat of fusion
J	index of the control volume containing the interface
k	thermal conductivity
K_M	kinetics coefficient
L	latent heat
q	heat flux
R	universal gas constant or radius of the wheel
t	time
Δt	time increment
T	temperature
T_0	substrate initial temperature
T_M	nominal equilibrium melting temperature
T_N	nucleation temperature
T_P	initial melt pouring temperature
ΔT_i	undercooling of the melt
V_0	characteristic atomic attachment velocity at the melting temperature
V_i	interface velocity
V_W	wheel surface linear velocity
x	spatial coordinate parallel to the substrate
X_D	detachment distance (from upstream meniscus of PFC)
y	spatial coordinate normal to the substrate
Δy	width of the control volume
Y_i	elevation of the solid/liquid interface above the substrate surface.

Greek symbols

α	thermal diffusivity
δ	distance of the solid/liquid interface from the center node
ρ	density.

Subscripts

i	interface
j	spatial index
L	liquid
S	solid
SB	sample bottom surface
SS	substrate surface
WS	wheel surface.

Superscript

n	time index.

We have developed for this purpose a modified interface tracking method based on Control Volume Integrals (CVI). We also use a volume element subdivision similar to that by Goodrich [12] but with a different node placement. Our CVI approach is effective for rapid solidification with and without undercooling. It can track accurately the interface and can predict the temperature of the interface during recalescence. We illustrate the numerical approach with models of two rapid solidification processes: Planar Flow Casting and Splat Cooling.

2. FORMULATION OF THE PHYSICAL PROBLEM

A brief description of the equations and physical characteristics of a simple one-dimensional solidification problem is given here. As will be discussed later, both the Planar Flow Casting and the Splat Cooling processes can be approximated in some cases by this model.

Let us assume that a thin layer of motionless molten metal is suddenly put in contact with a much colder substrate at time $t = 0$. The melt will then solidify. If there is no relative motion and if the deposited layer (the 'sample') is thin, we can approximate the heat transfer in the layer and in the substrate by one-dimensional conduction, for which the equation (with constant properties) is

$$\frac{\partial T_j}{\partial t} = \frac{\partial}{\partial y}\left(\alpha_j \frac{\partial T_j}{\partial y}\right) \tag{1}$$

where T is the temperature, t the time, y the vertical coordinate (normal to the substrate surface), and α the thermal diffusivity. The subscript j stands here either for 'S' (i.e. denoting the solid sample), 'L' (the liquid sample), or 'W' (the substrate, e.g. a wheel or solid wall). We use the convention that $y = 0$ at the substrate/melt interface, and that $y > 0$ for the sample.

The thermal contact between the sample and the substrate is quantified by a heat transfer coefficient h defined as

$$h = \frac{q_W}{T_{SB} - T_{WS}} \tag{2}$$

where q_W is the heat flux per unit area and per unit time between the sample and the substrate; and T_{SB} and T_{WS} are the temperature of the sample bottom

and of the substrate surface, respectively. This heat flux is also

$$q_W = -k_j \frac{\partial T_j}{\partial y}\bigg|_{y=0} \tag{3}$$

where subscript j stands either for the sample or substrate.

Some other boundary and initial conditions are also used. The substrate temperature far away from the sample is assumed to remain at room temperature T_0

$$T[y = -\infty, t] = T_0. \tag{4}$$

The sample and substrate are assumed to be initially at uniform temperatures equal to the pouring temperature and to room temperature, respectively

$$T[y > 0, t = 0] = T_P \tag{5}$$

and

$$T[y < 0, t = 0] = T_0. \tag{6}$$

An energy balance condition must also be satisfied at the solid/liquid interface

$$\rho_S L \frac{dY_i}{dt} = k_S \frac{\partial T_S}{\partial y}\bigg|_i - k_L \frac{\partial T_L}{\partial y}\bigg|_i \tag{7}$$

where Y_i is the elevation of the interface; the gradients are calculated at this interface; L is the latent heat of solidification; ρ_S the solid density; and k_S and k_L the thermal conductivities of the solid and liquid. The interface velocity is then

$$V_i = \frac{dY_i}{dt}. \tag{8}$$

An additional condition must be prescribed at the interface, and depends on the process:

(i) *Solidification without undercooling*

If there is no undercooling, the solidification will take place at a constant temperature (T_M) for a pure metal, and the additional boundary condition at the interface is

$$T[y = Y_i, t] = T_M. \tag{9}$$

The interface velocity is then directly determined by the energy balance at the interface (equation (7)), and depends on the temperature gradients at that location.

(ii) *Solidification with undercooling*

With undercooling a different approach must be used. Assuming heterogeneous nucleation and no nucleation barrier, the solidification rate depends on molecular mechanisms, and a well-known model for crystal growth in a pure melt is [13]

$$V_i = V_0 \exp\left[-\frac{E_V}{RT_M}\frac{\Delta T_i}{T_i}\right]\left[1 - \exp\left[-\frac{\Delta H_M}{RT_M}\frac{\Delta T_i}{T_i}\right]\right] \tag{10}$$

where V_0 is a molecular attachment velocity, E_V an activation energy, R the universal gas constant, ΔH_M the heat of fusion, T_M the equilibrium melting temperature, T_i the interface temperature, and ΔT_i the interface undercooling

$$\Delta T_i = T_M - T_i. \tag{11}$$

For small undercooling, equation (10) reduces in the first approximation to [8, 9]

$$V_i = K_M(T_M - T_i) \tag{12}$$

where the proportionality factor, K_M, is called the kinetics coefficient. We have, therefore, two unknown parameters at the interface in the case of solidification with undercooling: the interface velocity and the temperature, and we need two equations expressing the conditions at that location. These are the energy balance (equation (7)) and the kinetics relationship (equation (12)).

It is essential to note at this point that it is incorrect to assume that the interface temperature will return to the melting temperature after recalescence if the solidification kinetics are introduced in the model (via equation (12)). Indeed, this equation would then give a zero interface velocity if one assumes that $T_M = T_i$, which would be incompatible with the fact that the interface must move under control of the external heat transfer. In reality, the interface will reach a temperature below (but in the case of low heat transfer coefficients, approximately constant and close to) the equilibrium melting point (see Fig. 8). This small quasi-equilibrium level of undercooling is precisely that which corresponds (via equation (12)) to the interface velocity determined by the external thermal conditions (via equation (7)). This situation results, of course, from the strong coupling between the kinetics and the temperature field. Contrarily to what one might think at first, there is therefore no need nor reason to resort to an artificial switch from a model incorporating equations (7) and (12) to a model that includes instead equations (7) and (9) as the solidification shifts over time from being kinetically controlled to being thermally controlled. In other words, this 'shift' is already taken into account automatically in the coupling between the kinetics and the temperature field, and the results reflect therefore, at all times, a compromise between the two control mechanisms.

3. NUMERICAL TECHNIQUE AND INTERFACE TRACKING

The system described above is a one-dimensional phase change problem with moving interface, and several numerical methods have been used to solve this type of problem [3–6]. In the present work, a CVI method [14, 15] is combined with volume element subdivision to track the interface and to predict its velocity and temperature.

The sample and substrate regions are both represented by a uniform finite difference grid, but the

node spacing in the substrate and in the sample may be different. The finite difference equations for the nodal temperatures are obtained directly by integration of the differential energy equation from time (t) to $(t+\Delta t)$ and over each control volume from $-\Delta y/2$ to $\Delta y/2$. For control volume j in the sample or in the substrate we have

$$\int_t^{t+\Delta t}\int_{-\Delta y/2}^{\Delta y/2}\frac{\partial T}{\partial t}\,dy\,dt=\int_t^{t+\Delta t}\int_{-\Delta y/2}^{\Delta y/2}\frac{\partial}{\partial y}\left(\alpha\frac{\partial T}{\partial y}\right)dy\,dt \tag{13}$$

or

$$\int_t^{t+\Delta t}\int_{-\Delta y/2}^{\Delta y/2}\frac{\partial T}{\partial t}\,dy\,dt=\Delta t\left[\left(\alpha_{j+1/2}\frac{\partial T}{\partial y}\bigg|_{\Delta y/2}\right)-\left(\alpha_{j-1/2}\frac{\partial T}{\partial y}\bigg|_{-\Delta y/2}\right)\right]. \tag{14}$$

The implicit difference equation can be written as

$$(T_j^{n+1}-T_j^n)\Delta y=\Delta t\left[\left(\alpha_{j+1/2}\frac{T_{j+1}^{n+1}-T_j^{n+1}}{\Delta y}\right)-\left(\alpha_{j-1/2}\frac{T_j^{n+1}-T_{j-1}^{n+1}}{\Delta y}\right)\right] \tag{15}$$

and reorganized as

$$a(j)T_j^{n+1}=b(j)T_{j+1}^{n+1}+c(j)T_{j-1}^{n+1}+d(j) \tag{16}$$

where

$$a(j)=1+b(j)+c(j) \tag{17}$$

$$b(j)=\frac{\alpha_{j+1/2}\Delta t}{\Delta y^2} \tag{18}$$

$$c(j)=\frac{\alpha_{j-1/2}\Delta t}{\Delta y^2} \tag{19}$$

$$d(j)=T_j^n. \tag{20}$$

In these equations, subscripts j, $j+1$, and $j-1$ represent the nodes at the center of the respective control volume, whereas $j+1/2$ and $j-1/2$ indicate the two boundaries of the jth volume. The superscripts n and $n+1$ are successive time indexes. Δy is the height of the control volume and Δt the time step.

A special treatment is adopted for the control volume containing the moving interface. In an approach similar to Goodrich's [12], the Jth control volume encompassing the interface is divided into two smaller ones separated by the interface, one solid (J_S) and one liquid (J_L). In our case, however, new nodes are then introduced at the center of each of these new volumes as well as on the interface itself for improved accuracy. Two additional difference equations for T_{JS} and T_{JL} are then obtained by integrating equation (1) over each smaller volume. Different approaches for the tracking of the interface must be used depending on whether there is undercooling or not.

(i) *Interface tracking without undercooling*

The interface is treated as a zero thickness volume kept at T_M. The new position of the interface is directly calculated from the interface energy balance equation (7) with the temperature gradients differenced by using the temperature T_{JS}, T_{JL} and T_M at the previous time step. The equation is

$$Y_i^{n+1}=Y_i^n+c_1(T_M-T_{JS}^n)+c_2(T_M-T_{JL}^n) \tag{21}$$

in which c_1 and c_2 are

$$c_1=\frac{2\Delta t k_S}{\rho_S L\left(\frac{\Delta y}{2}-\delta\right)} \tag{22}$$

and

$$c_2=\frac{2\Delta t k_L}{\rho_S L\left(\frac{\Delta y}{2}+\delta\right)} \tag{23}$$

with

$$\delta=y_J-Y_i^n \tag{24}$$

which is the distance between the interface (Y_i) and the center (y_J) of the volume element where it is located. After computation of the interface position at the current time step, the temperatures can be calculated by solving equations (16) and the equations for T_{JS} and T_{JL} using a tri-diagonal matrix algorithm (TDMA) [16]. The calculation of the interface position is therefore explicit whereas the node temperatures are computed implicitly.

(ii) *Interface tracking with undercooling*

In this case, the interface velocity can be explicitly calculated using the kinetics relationship (equation (12)) expressed at the previous time step

$$V_i^n=K_M(T_M-T_i^n). \tag{25}$$

The interface position at the new time is then

$$Y_i^{n+1}=Y_i^n+V_i^n\Delta t. \tag{26}$$

T_i^{n+1} can be determined implicitly with the interface energy equation (7)

$$(c_1+c_2)T_i^{n+1}=c_1T_{JS}^{n+1}+c_2T_{JL}^{n+1}+V_i^n\Delta t \tag{27}$$

where c_1 and c_2 are those given above. After having calculated the new interface position it is then possible to determine all the nodal temperatures including the new interface temperature by solving the full system of implicit equations using the TDMA approach.

With and without undercooling, an approach similar to that used at the interface is used to treat the temperature jump between the sample and the substrate surface. Two zero-thickness volume elements are introduced at the sample bottom and substrate surface, respectively. At each of these surfaces, boundary condition (3) is used, and the two resulting implicit

finite difference equations involve the surface temperatures and those of the neighboring nodes. In addition, finite difference equations are generated in the substrate as well because we have shown [17] that it is important to include the heat transfer in the substrate in numerical models of rapid solidification processes based on direct contact with a cold substrate.

It is worth emphasizing here the reason why an element subdivision approach was used in this work. Such an approach would already result in increased resolution of the interface tracking for modelling of basic equilibrium (no undercooling) phase change problems. (Indeed, without subdivision the entire element containing the interface is assumed to be either fully-solid or fully-liquid, with correspondingly limited resolution.) However, the element subdivision technique takes a particular significance for modelling of phase change with undercooling. In this case, as mentioned above, the interface temperature becomes unknown a priori and must be calculated. It therefore makes more sense physically to model the interface as a 'separate entity' with its own temperature (which is what we are doing with our subdivision technique) rather than to lump it together either with a fully-solid or fully-liquid element (as one does without this subdivision approach). In our model, we subdivide the element containing the interface into three separate regions: solid, liquid, and interface itself, each with a specific node, distinct properties, and—most importantly—each with a distinct temperature. The latter point distinguishes our approach from most previous ones which treated the interface temperature as the average temperature of the whole element containing the interface (i.e. encompassing both the solid and liquid fractions).

The fact that the interface temperature is calculated separately is very important for modelling of solidification with undercooling. Indeed, such treatment will result in a much more accurate interface temperature prediction and in turn more accurate calculations of interface velocities, interface location, latent heat releases, and temperature distribution. We believe, therefore, that our subdivision approach is particularly well-suited for modelling of solidification with large undercooling.

4. VALIDATION OF THE CVI TECHNIQUE AND IMPLEMENTATION FOR PLANAR FLOW CASTING

4.1. *Planar flow casting: problem statement*

To illustrate the treatment of solidification assumed without undercooling, we discuss here Planar Flow Casting (PFC), a process used for the rapid solidification of thin metal foils that uses a crucible positioned close to a spinning wheel. (There may in reality be undercooling during this process, but most models to date have neglected this aspect.) A schematic of the system is shown in Fig. 1. The molten metal in the crucible is forced through a nozzle and forms a 'solidification puddle' between the bottom of the crucible and the wheel surface. The melt solidifies upon contact with the wheel, and a thin foil is dragged by the wheel motion. Our experimental work has indicated [18] that the downstream meniscus detaches from the crucible bottom well away from the nozzle. Given the large aspect ratio of the melt puddle, and considering that the axial velocity is generally much greater than the normal velocity, it is therefore reasonable to approximate the melt puddle by a thin rectangular strip.

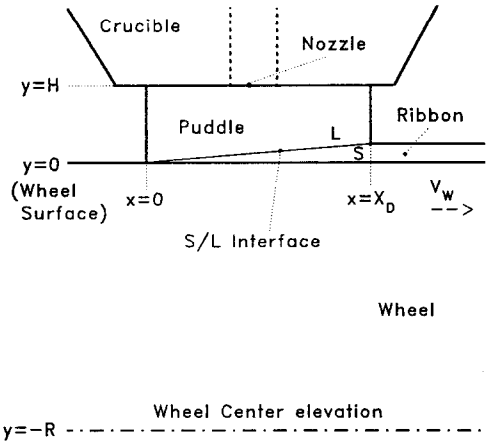

FIG. 1. Schematic of the Planar Flow Casting geometry and coordinate system used in the numerical model.

To simplify the model, we consider that there is no velocity gradient in the puddle. Clearly, this is not true in the actual case (as we have shown in our two-dimensional models [18, 19]). Our primary objectives here are to identify relative trends and to conduct parametric investigations, however, and we believe that such information can be obtained with a one-dimensional model.

Other simplifying assumptions have also been made:

(a) The overall flow field is assumed to be steady state.

(b) We limit ourselves to the study of the puddle under the crucible and of the wheel below the puddle.

(c) We neglect convective heat transfer normal to the wheel.

(d) Heat conduction parallel to the substrate surface is neglected in the first approximation.

(e) We consider solidification of a pure metal.

(f) We assume that local thermodynamic equilibrium exists at the solid/liquid interface (i.e. $T_i = T_M$).

(g) The initial temperature distributions of the substrate and of the puddle are assumed to be uniform at room temperature ($T_0 = 300$ K) and pouring temperature (T_p), respectively.

(h) The temperature at the top surface of the puddle is assumed to be maintained at the pouring temperature.

(i) The heat loss through the menisci is neglected.

(j) The curvature of the wheel is neglected and the wheel surface is assumed to be horizontal.

(k) A no-slip condition at the wheel surface is assumed.

(l) The material properties are assumed to be independent of temperature, but are different in the liquid and solid regions.

(m) Shrinkage during solidification is neglected.

With the coordinates depicted in Fig. 1 and these assumptions, the boundary layer energy equation becomes then (for constant properties)

$$V_W \frac{\partial T_j}{\partial x} = \frac{\partial}{\partial y}\left(\alpha_j \frac{\partial T_j}{\partial y}\right) \tag{28}$$

where V_W is the velocity of the wheel surface, x the distance parallel to the wheel surface, y the distance normal to the wheel surface, α_j the thermal diffusivity, and subscript 'j' stands either for L or S (i.e. it represents the liquid or the solidified layer). Because of the assumption that there is no relative motion within the melt, this two-dimensional steady-state boundary layer problem can be reduced to a one-dimensional unsteady-state heat conduction problem through a change of coordinate, and this equation becomes then the basic unsteady-state conduction equation discussed above (equation (1)). Most of the features of the generic solidification problem discussed above are applicable to this simplified PFC model, but we also use here the fact that the temperature profile should be symmetrical at the center of the wheel. We also assume that the heat transfer coefficient is constant whereas in reality it is likely to change with distance because of shrinkage and stresses in the solidifying metal.

4.2. *Validation of the CVI method and comparison with the enthalpy technique*

The validity of this implementation of the CVI method was confirmed by comparing it to the basic enthalpy technique [5]. Results such as the interface location or the temperature history in the puddle were generated by both methods and then compared. The same grid was used for both methods (200 nodes in the puddle which is 350 μm thick, and 200 nodes over 1000 μm in the wheel) for better comparison of the relative resolution of the two techniques. Different time steps had to be used to ensure stability of the schemes, however: 2.5×10^{-8} s for the CVI method and a smaller 5×10^{-9} s for the enthalpy method (which is fully explicit). The results are not shown here in the interest of brevity, but the overall agreement was excellent, which suggests that our implementation of the CVI technique is probably sound. It was seen, however, that for the same grid spacing the CVI method tracks the interface much more precisely because we subdivide the control volume where the interface is located. Naturally, it would be possible to use a much finer grid for the enthalpy method but this would entail a much longer calculation time, especially if stability has to be preserved. The standard enthalpy method could also be improved by interpolation within the volume element containing the interface [20], but may then involve solving more complicated differential equations. We are not aware at this time of any previous use of an enthalpy method with node subdivision for problems with undercooling. The present CVI approach certainly allows us to track easily the interface with very high resolution even for cases involving undercooling and recalescence (see below).

Table 1. Property values used in the computations

		Al	Steel	Cu
T_M	K	933	1809	
L	kJ kg^{-1}	395	272	
C_{PL}	J kg^{-1} K^{-1}	1200	691	
C_{PS}	J kg^{-1} K^{-1}	1060	691	503
k_L	W m^{-1} K^{-1}	100	34	
k_S	W m^{-1} K^{-1}	200	34	393
ρ_L	kg m^{-3}	2340	7400	
ρ_S	kg m^{-3}	2700	7400	9000

4.3. *Examples of numerical results and discussion*

Some results obtained for the PFC process with our CVI method are shown hereafter for illustration, in particular the effect of the thermal contact between the wheel and the puddle, a parameter of major importance for the solidification process.

The computations described in this article are based on our recent experimental data on PFC solidification puddle dynamics (the experimental procedures are described in detail elsewhere [21]). The parameters used are: wheel speed, 23 m s^{-1}; puddle height, 350 μm; superheat, 50 K; and puddle length (approximated by the distance to detachment from the crucible), 5.45 mm. The corresponding measured ribbon thickness is 68 μm. The properties used in the calculations are given in Table 1. Two hundred nodes were used both in the puddle and in the wheel. The calculation domain in the wheel was 1000 μm for the copper wheel, which is sufficient given the small thermal penetration depth achieved during the short wheel residence time under the puddle (about 0.25 ms).

Figure 2 shows the calculated solid/liquid interface position as a function of the distance from the upstream meniscus for various puddle/wheel heat transfer coefficients when spinning aluminum on a copper wheel with the process parameters given above. These results take into account the heat transfer within the wheel itself. The crucible detachment distance (X_D) is defined as the distance from the upstream meniscus to the point where the melt detaches from the crucible bottom surface, and constitutes the downstream limit

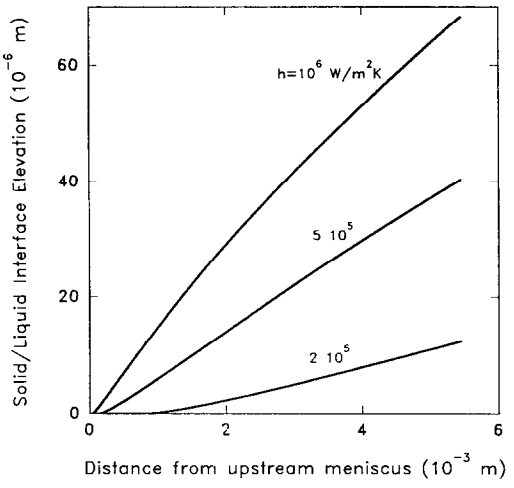

FIG. 2. Interface location as a function of distance from the upstream meniscus for aluminum spun on a copper wheel. Heat transfer coefficients: 2×10^5, 5×10^5, and 10^6 W m^{-2} K^{-1}. (Gap = 350 μm, V_W = 23 m s^{-1}, $T_P - T_M$ = 50 K, T_0 = 300 K, X_D = 5.45 mm, ribbon thickness = 68 μm.)

of these calculations. It can be seen in this graph that the computed thickness of the solidified layer is approximately equal to the measured final ribbon thickness (68 μm) at the detachment distance if a value of 10^6 W m^{-2} K^{-1} is used for the heat transfer coefficient at the wheel. This implies that the ribbon would be already completely solidified within the boundaries of the puddle for this particular thermal contact condition. In other words the ribbon formation is subject to 'thermal control' in the puddle.

On the other hand, when the thermal contact between puddle and wheel surface is poorer, for $h = 2\times10^5$ W m^{-2} K^{-1} for example, the solidified thickness would only be 12 μm at the crucible detachment point. This indicates that most of the layer dragged out of the puddle consists of still-liquid melt, and that the puddle length and the ribbon formation are primarily determined by the fluid flow (i.e. by the momentum boundary layer) in the puddle [22]. This is the 'momentum control' case during which solidification is completed well out of the puddle. In this case, a Newtonian cooling model (i.e. assuming uniform temperature) is sometimes used as a first approximation to study the ribbon solidification process if the Biot number is small enough [23]. Besides poor thermal contact, momentum-controlled ribbon formation could also result from delays in nucleation, in which case we would have a departure from isothermal solidification in local equilibrium, i.e. undercooling, which we are not considering in the present case.

The extent to which heat or momentum transfer will be the controlling factor for the ribbon solidification depends of course greatly on the thermal contact between the puddle and the wheel. This parameter is affected by the choice of the melt and wheel materials, the wetting characteristics of the melt and the wheel surface [24], the surface condition of the wheel [25], and the wheel surface velocity [26], among others. Variations in thermal contact will therefore result in different cooling and solidification characteristics. To illustrate further this effect, Fig. 3 shows the cooling rate of the liquid melt at the interface, and Fig. 4 shows the interface velocity in the puddle, both for three different values of the heat transfer coefficient at the wheel surface. (In these figures, we are using the *vertical* axis to represent the *vertical* distance from

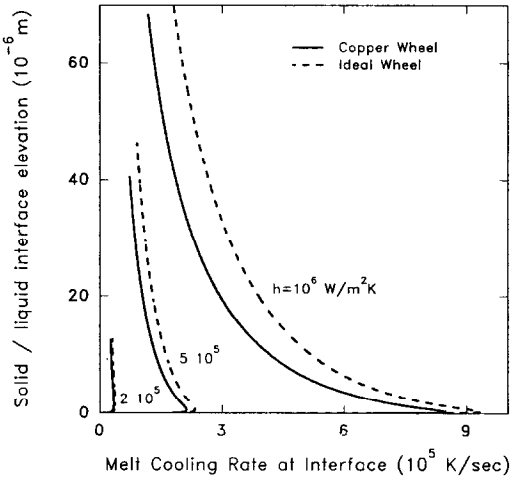

FIG. 3. Local melt cooling rate at the interface as a function of distance from the wheel for aluminum spun on Cu and ideal wheels. Heat transfer coefficients: 2×10^5, 5×10^5, and 10^6 W m^{-2} K^{-1}. (Gap = 350 μm, V_W = 23 m s^{-1}, $T_P - T_M$ = 50 K, T_0 = 300 K, X_D = 5.45 mm, ribbon thickness = 68 μm.)

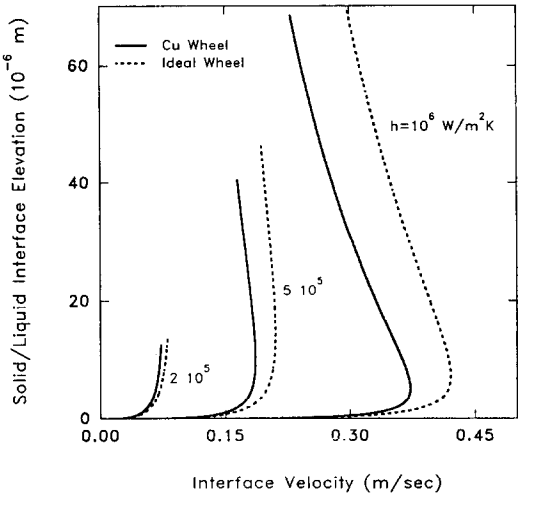

FIG. 4. Interface velocity as a function of distance from the wheel for aluminum spun on copper and ideal wheels. Heat transfer coefficients: 2×10^5, 5×10^5, and 10^6 W m^{-2} K^{-1}. (Gap = 350 μm, V_W = 23 m s^{-1}, $T_P - T_M$ = 50 K, T_0 = 300 K, X_D = 5.45 mm, ribbon thickness = 68 μm.)

the wheel surface, and the horizontal axis for the parameter of interest. The curves are limited to the height corresponding to the solidified thickness at the detachment point.) The solid lines correspond to the calculations for a copper wheel, whereas the dashed lines are for a hypothetical ideal isothermal wheel that would remain at its initial temperature at all times. The melt cooling rate at the interface is calculated here by

$$\dot{T}_i = \left.\frac{\partial T}{\partial y}\right|_{i,L} V_i \tag{29}$$

where the temperature gradient is computed at the interface on the liquid side, and V_i is the solid/liquid interface velocity. Both of these quantities are of great importance to the materials scientist conducting microstructural investigations of ribbons produced by this rapid solidification technique.

As expected, these figures illustrate the fact that higher interface cooling rate and interface velocity are achieved for a higher value of the heat transfer coefficient. It can be seen that both the interface velocity and the interface cooling rate at high heat transfer coefficients decrease significantly as the interface moves away from the wheel. This decrease results from the additional heat transfer resistance introduced by the growing solid layer through which the released latent heat must be conducted away. This resistance plays a proportionally greater role for large heat transfer coefficients at the wheel, which explains the faster decrease in cooling rate in this case.

The decrease in interface cooling rate with increasing distance from the wheel is also seen if one considers the thermal history of the ribbon in Fig. 5 which shows

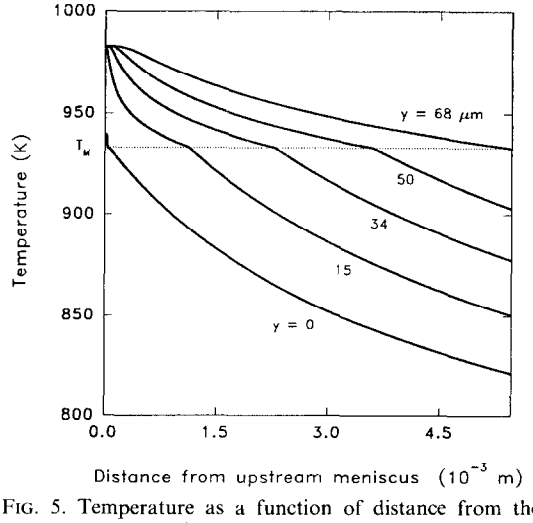

FIG. 5. Temperature as a function of distance from the upstream meniscus for aluminum spun on a copper wheel. Distance from the wheel: 0 (bottom of puddle), 15, 33, 50, and 68 (top of ribbon) μm. ($h = 10^6$ W m^{-2} K^{-1}, gap = 350 μm, $V_W = 23$ m s^{-1}, $T_P - T_M = 50$ K, $T_0 = 300$ K, $X_D = 5.45$ mm, ribbon thickness = 68 μm.)

the calculated temperature as a function of distance from the upstream meniscus (i.e. as a function of time) at several heights in the puddle for $h = 10^6$ W m^{-2} K^{-1}. The top curve in the figure corresponds to the final ribbon thickness (i.e. to the ribbon top surface) and the bottom curve corresponds to the puddle (and ribbon) bottom. Intermediate heights have been identified by their distance from the wheel surface. The melting temperature is indicated by a horizontal line for reference, and shows when solidification takes place at any given height in the puddle. The gradient of the curves on the liquid (upper) side of the interface is related to the interface cooling rate as defined in equation (29). Clearly, this gradient depends on the height, and is seen to decrease as the vertical distance from the wheel increases, in agreement with Fig. 3.

Figures 3 and 4 also illustrate the effect of the heat transfer in the wheel on the interface velocity and cooling rate. It is commonly assumed in melt-spinning (and other) models that the substrate temperature remains constant. This situation corresponds here to the curves for an ideal wheel of infinite heat capacity and thermal conductivity. It is easily seen, however, that significant differences in cooling rate and interface velocity exist between calculated results for an ideal wheel and for a copper wheel assumed to have a more realistic heat transfer behavior. This observation suggests that numerical models for rapid solidification should indeed include wheel heating for more accurate calculations of cooling rates and interface velocities. (In fact, we have shown that the wheel surface temperature may increase by several hundred Kelvin under the solidification puddle, even for a copper wheel [17].) It should be noted that the wheel heating effect is linked to the fact that rapid solidification processes involve large amounts of energy transferred over small periods of time. If the process was to be much slower, the wheel surface would not heat up as much because of greater thermal penetration in the wheel, and the surface heating effect on solidification would then be smaller. Interestingly, having the wheel water-cooled internally would generally not prevent this large heating which does occur only over a very thin layer in the wheel and may therefore not affect the inner rim temperature. Water cooling will take care of overall heating of the wheel over long periods of time, on the other hand.

As expected, the interface cooling rate and interface velocity are smaller for the 'realistic' wheel than for the 'ideal' wheel because the wheel surface temperature increases in the former case, and this increase does in turn decrease the heat transfer through the wheel surface (equation (2)). Also expected is the fact that the difference between the actual and the ideal wheel increases with an increase in the heat transfer coefficient. This is because for a higher heat transfer coefficient there is more energy transferred to the wheel per unit time than in the case of a low heat transfer coefficient. If the wheel is nonideal, its finite thermal diffusivity will prevent the rapid transfer of

this energy towards the center of the wheel, which in turn keeps the surface temperature very high, and will lead to a large departure from the ideal isothermal case. For the low heat transfer coefficients, however, the energy flux per unit time is smaller, and less energy accumulates close to the surface because a proportionally greater share can diffuse towards the center, which in turn keeps the surface temperature lower, i.e. closer to ideal isothermal conditions.

Figure 3 shows that large variations of interface cooling rate exist across the ribbon section for high heat transfer coefficients. For $h = 10^6$ W m^{-2} K^{-1}, for example, the interface cooling rate close to the wheel surface reaches 8×10^5 K s^{-1} for the copper wheel. At the top of the ribbon, on the other hand, an interface cooling rate of only 10^5 K s^{-1} is achieved, approximately one order of magnitude difference. This difference is perhaps large enough to contribute to the significant variations in microstructure that are observed across ribbons produced by PFC. The variation in cooling rate is reduced for poorer thermal contact between the puddle and the wheel because the correspondingly smaller heat flux results in smaller temperature gradients within the puddle.

Figure 4 shows the variations of interface velocity within the puddle. As in the case of interface cooling rate, the interface velocity appears to be high relatively close to the wheel and decreases as the interface moves far away from the wheel. For $h = 10^6$ W m^{-2} K^{-1}, for example, the variation of the interface velocity across the ribbon thickness ranged from about 0.38 m s^{-1} close to the wheel surface to about 0.23 m s^{-1} at the top surface of the ribbon. This variation—when combined with the steep temperature gradients present close to the wheel for high heat transfer coefficients—results in the large variations in interface cooling rate across the ribbon that are mentioned above.

It is interesting to note, however, that the interface velocity in fact increases at first as the interface starts to grow inside the puddle. After the interface has penetrated a short distance, its velocity reaches a maximum and then decreases again, as mentioned above. This initial increase in interface velocity is probably related to the melt superheat. Indeed, in the earliest stages of the solidification process, only a thin layer of liquid above the interface is cooled down from the superheated state. This probably results in a steep localized temperature gradient on the liquid side of the interface, and therefore in a relatively low interface velocity because of conduction from the liquid side to the interface. After a while, however, the superheat is reduced in a thicker layer above the interface, therefore resulting in a smaller temperature gradient in that region and in an increasing velocity. A counterbalancing effect is that the solidified layer constitutes an increased resistance to conduction as the interface penetrates further in the puddle. This increased resistance would result in a decrease in heat extracted which in turn leads to a lower interface velocity. The velocity maximum observed might then result from the combination of these two opposite effects, the superheat effect being dominant very close to the wheel and the resistance to conduction effect taking over for greater distances.

A more detailed investigation of the effect of a number of parameters (such as the heat transfer in the wheel, the wheel material, the local wheel surface heating, the melt superheat, and the melt material) on the solidification characteristics can be found elsewhere [17].

5. APPLICATION TO SOLIDIFICATION WITH UNDERCOOLING: SPLAT COOLING

We present here for illustration some results obtained with our CVI model for the case of the rapid solidification with undercooling that may take place during the splat cooling process.

5.1. *Problem statement*

Splat cooling is a generic term that is often used to designate the solidification of droplets of molten metal suddenly contacting a cold substrate. The drops may be allowed to fall by gravity onto a horizontal substrate, may be sprayed onto a surface (the 'spray forming' process), or may be squeezed between two surfaces (the 'hammer-and-anvil' and the 'two-hammers quencher'). In the following discussion, we consider a simple model of these processes that consists of a very thin layer of motionless molten metal being suddenly placed in contact with a horizontal substrate. The cooling of the melt is very fast if the melt layer is thin and if the thermal contact between the sample and substrate is good; such a situation will often result in significant undercooling.

We are addressing here the case of a pure aluminum splat on a copper substrate. The splat is assumed to be 50 μm thick and originally superheated uniformly by 50 K. (The property values used here are given in Table 1.) The copper substrate is assumed to be at a uniform room temperature ($T_0 = 300$ K) before contact (at $t = 0$). We are considering here the case of solidification with melt undercooling, and we assume for simplicity that nucleation takes place at a set undercooling level. We also consider that there is no nucleation barrier after nucleation, and that the solidification front is planar. We use in the first approximation a linear kinetics relationship (equation (12)) between the interface velocity and the undercooling at the interface. The kinetics coefficient K_M is taken to be $K_M = 0.05$ m s^{-1} K^{-1} for pure aluminum [8, 9]. The boundary conditions used are that the upper surface of the splat is adiabatic (i.e. we neglect radiation and convection) and that the temperature far away within the substrate remains at room temperature. We assume property values that are independent of temperature, but different in the liquid and solid splat layers. We neglect shrinkage during solidification. We consider that the splat is of uniform

thickness and is much wider than it is thick. Conduction parallel to the substrate surface is then neglected and we can assume a one-dimensional problem.

With these assumptions, the splat cooling process is then represented by a simple one-dimensional unsteady-state conductive heat transfer model as described in Section 2 above. We show hereafter some results to illustrate the implementation of the CVI technique for the tracking of the interface during cases of high undercooling and recalescence.

5.2. *Numerical results*

The CVI numerical technique described above has been used for the modelling of splat cooling with undercooling. As discussed previously, the departure from equilibrium at the interface introduces an extra degree of freedom: the unknown interface temperature. This unknown is determined through the use of the kinetics relationship between the interface velocity and the interface undercooling.

Figure 6 shows the temperature profile in the splat at various times after contact of the splat with the substrate ($h = 10^6$ W m^{-2} K^{-1}, 100 K undercooling, $K_M = 0.05$ m s^{-1} K^{-1}). It can be seen that the temperature of the melt at the bottom of the splat dropped down to our set nucleation temperature (833 K, i.e. 100 K undercooling) after 17 μs. The whole splat is still liquid at this point, and it can also be noted that the top surface of the splat remains superheated by about 20 K. At that instant the melt nucleates on the substrate surface, and the solid/liquid interface begins to move inside the splat. To illustrate this effect, three additional temperature profiles in the splat are also shown for later times. These times were chosen to correspond to three specific solidified fractions of the splat: 20 μs (corresponding to $f_s = 0.05$, i.e. 5% of the splat has solidified), 98 μs ($f_s = 0.7$), and 144 μs ($f_s = 1$). After 20 μs, it can be seen that the interface has penetrated about 2 μm inside the splat, and its position is indicated by a local temperature maximum. This maximum is caused by the fact that the large undercooling induces a high interface velocity, which in turn corresponds to the liberation of a great amount of latent heat. This energy release is too large and too fast for all of the energy to be conducted away to the substrate, and the melt is therefore heated up locally. Naturally, energy is conducted in both directions, and the undercooled melt above the interface is heated up as well. As the still-undercooled melt heats up, the interface velocity decreases significantly, which in turn means less latent heat released, and the local temperature maximum disappears as soon as all the latent heat can be promptly transferred directly to the substrate. At 98 μs, for example, the interface is located at 35 μm from the substrate ($f_s = 0.7$), and a maximum is no longer visible. Interestingly, the melt above the interface on the top part of the splat is now undercooled as well, but shows no variation of temperature. The temperature gradient in the solid layer is about uniform at that time (because aluminum has a high thermal conductivity). After 144 μs, the splat is entirely solidified, and the temperature profile is still approximately linear. These results agree qualitatively with the numerical results obtained by Clyne [9] with his heat source model.

The calculated interface velocity is shown in Fig. 7 for three heat transfer coefficients (10^5, 10^6, and 10^7 W m^{-2} K^{-1}). As expected, the velocity is generally larger for a larger heat transfer coefficient (i.e. greater heat flux), except very close to the substrate where

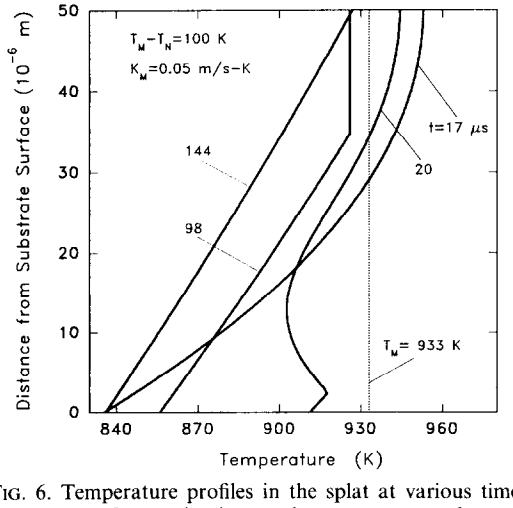

FIG. 6. Temperature profiles in the splat at various times after contact for an aluminum splat on a copper substrate: $t = 17$, 20, 98, and 114 μs. ($h = 10^6$ W m^{-2} K^{-1}, $T_N = 833$ K, $K_M = 0.05$ m s^{-1} K^{-1}, splat thickness = 50 μm, $T_P - T_M = 50$ K, $T_0 = 300$ K.)

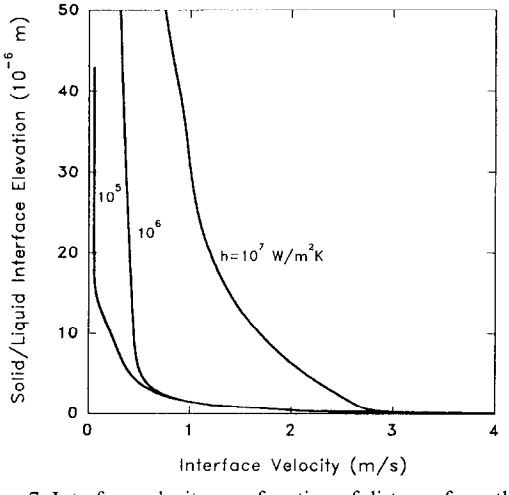

FIG. 7. Interface velocity as a function of distance from the substrate for an aluminum splat on a copper substrate (with undercooling). Heat transfer coefficients: 10^5, 10^6, and 10^7 W m^{-2} K^{-1}. ($T_N = 833$ or 100 K initial undercooling, $K_M = 0.05$ m s^{-1} K^{-1}, splat thickness = 50 μm, $T_P - T_M = 50$ K, $T_0 = 300$ K.)

this velocity appears to be independent of the heat flux into the substrate. This is because in that domain the interface velocity is controlled by the fast kinetics (because of the large undercooling), with essentially no influence of the heat transfer to the substrate. As soon as the interface has penetrated further into the splat, the external heat transfer begins to limit the rate of energy extraction, and the interface slows down significantly. It should indeed be noted that the velocity is of course dependent on the heat fluxes (see equation (7)) in addition to being a function of the undercooling, or in other words, that the level of undercooling is coupled to the heat fluxes through the intermediary of the interface velocity. The thermal contact at the substrate is therefore the primary control of the interface velocity after recalescence.

The interface temperature variation as a function of interface position is given in Fig. 8 for the same conditions as those of Fig. 7. The calculated interface temperature is shown for the same three heat transfer coefficients. (The shape of these curves is in fact a mirror image of those for the interface velocity because of the nature of equation (12).) As expected, the interface temperature remains lower overall (i.e. the undercooling is larger) for higher h values except immediately next to the substrate. The interface temperature increases rapidly during the recalescence process close to the substrate, followed by a slower increase further away. We can see that the interface temperature never becomes exactly equal to the equilibrium melting temperature, even for the lowest heat transfer coefficient. Instead, it reaches a quasi-steady equilibrium interface temperature of just a few Kelvin below the nominal equilibrium melting temperature in the upper half of the splat. This approximately

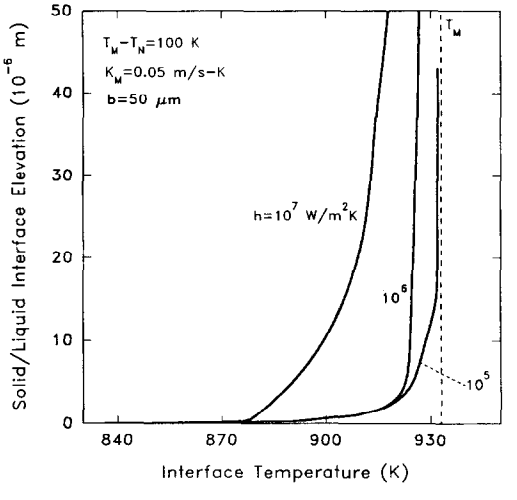

FIG. 8. Interface temperature as a function of distance from the substrate for an aluminum splat on a copper substrate (with undercooling). Heat transfer coefficients: 10^5, 10^6, and 10^7 W m^{-2} K^{-1}. (T_N = 833 or 100 K initial undercooling, K_M = 0.05 m s^{-1} K^{-1}, splat thickness = 50 μm, $T_P - T_M$ = 50 K, T_0 = 300 K.)

constant interface undercooling corresponds to the quasi-steady interface velocity seen in Fig. 7 for low heat transfer coefficient. It depends strongly on the external heat transfer, and is an important characteristic of the process. The value of this 'minimum undercooling' will determine, for example, if desirable metastable states or effects can be achieved in the upper region of the splat for the given process conditions.

The results on splat solidification shown here were intended to illustrate the use of the improved CVI method on problems with undercooling. A more extensive investigation of the splat cooling process has also been conducted with this model, and many additional results on the temperature profiles, the variations of interface temperature, the temperature history at various locations in the splat, the effect of the melt or substrate material, the effect of the undercooling level and the kinetics rate, and the interface cooling or heating rate can be found in other articles [27, 28].

6. CONCLUSIONS

We have developed a simple numerical approach to the modelling of heat transfer and phase change during rapid solidification processes without and with undercooling. In the latter case, this model takes into account crystal growth kinetics, but otherwise the numerical schemes are identical, which simplifies the programming considerably. Our approach is based on a modified interface tracking finite difference method implemented through a CVI technique. Both high computational efficiency, high resolution, and high accuracy are obtained through subdivision of the volume element containing the solid/liquid interface and through separate treatment of the solidification interface. This technique allows us to calculate much more precisely the interface position, cooling rate, and velocity. For the case of solidification with undercooling, the method can also predict the large variation of interface temperature during recalescence without problems due to numerical instability. The approach was found to be simple to implement and very effective, and the results were found to be of higher resolution—but in very good agreement otherwise—than those obtained for solidification without undercooling with a model based on the enthalpy technique.

Using the improved CVI technique, we were able to develop a simple model of the heat transfer and phase change taking place during the PFC process. The model also includes the heat transfer in the wheel, and takes into account the large wheel surface heating effect that in turn slows down significantly the solidification process. The influence of the heat transfer coefficient at the wheel surface on the interface cooling rate and on the interface velocity was quantified. The interface velocity and interface cooling rate were seen to decrease significantly when far away from the wheel surface. It was also observed that the interface velocity

shows a maximum close to the wheel surface, probably due to the superposition of superheat and conduction resistance effects.

This numerical model can also be readily used for the investigation of systems with high undercooling, and we were able to study quantitatively the recalescence and solidification during splat cooling. The temperature profiles in the splat can be computed as a function of time, and show local temperature inversions. The interface velocity was also calculated and showed very large variations across the splat that are, in general, strong functions of the substrate heat transfer coefficient, except immediately next to the substrate, where this velocity appeared to be primarily controlled by kinetics. For low heat transfer coefficients, the interface temperature reaches after recalescence a quasi-steady minimum undercooling level close to the nominal melting point.

We believe that this numerical technique is particularly simple and effective for heat transfer modelling of rapid solidification processes with undercooling.

Acknowledgements—We gratefully acknowledge partial support by the National Science Foundation (grant No. MSS-8957733) and by the Defense Advanced Research Projects Agency (contract No. N00014-86-K0753). We would also like to thank Prof. W. Lick (UCSB) for very valuable discussions on numerical modelling techniques.

REFERENCES

1. L. I. Rubenstein, *The Stefan Problem*. American Mathematical Society, Providence, Rhode Island (1971).
2. H. Jones, A comparison of approximate analytical solutions of freezing from a plane chill, *J. Inst. Metals* **97,** 38–43 (1969).
3. V. J. Lunardini, *Heat Transfer in Cold Climates*. Van Nostrand Reinhold, New York (1981).
4. J. Crank, *Free and Moving Boundary Problems*. Clarendon Press, Oxford (1984).
5. S. Fukusako and N. Seki, Fundamental aspects of analytical and numerical methods on freezing and melting heat transfer problems, *A. Rev. Numer. Fluid Mech. Heat Transfer* **1,** 351–402 (1988).
6. D. Poirier and M. Salcudean. On numerical methods used in mathematical modeling of phase change in liquid metals, *J. Heat Transfer* **110,** 562–570 (1988).
7. P. H. Shingu and R. Ozaki, Solidification rate in rapid conduction cooling, *Metall. Trans. A* **6A,** 33–37 (1975).
8. C. G. Levi and R. Mehrabian, Heat flow during rapid solidification of undercooled metal droplets, *Metall. Trans. A* **13A,** 221–234 (1982).
9. T. W. Clyne, Numerical treatment of rapid solidification, *Metall. Trans. B* **15B,** 369–381 (1984).
10. M. G. Chu, A. Giron and D. A. Granger, Microstructure and heat flow in melt-spun aluminum alloys, *Proc. 1986 Int. Conf. on Rapidly Solidified Materials*, pp. 311–316. American Society for Metals, Metals Park, Ohio (1986).
11. H. H. Liebermann, Rapidly solidified alloys made by chill block melt-spinning processes, *J. Crystal Growth* **70,** 497–506 (1984).
12. L. E. Goodrich, Efficient numerical technique for one-dimensional thermal problems with phase change, *Int. J. Heat Mass Transfer* **21,** 615–621 (1978).
13. C. G. Levi, The evolution of microcrystalline structures in supercooled metal powders, *Metall. Trans. A* **19A,** 699–708 (1988).
14. S. V. Patankar, *Numerical Heat Transfer and Fluid Flow*. Hemisphere, New York (1981).
15. W. J. Lick, *Difference Equations from Differential Equations*, Lecture Notes in Engineering, Vol. 41. Springer, New York (1989).
16. S. V. Patankar, Parabolic systems: finite-difference method I. In *Handbook of Numerical Heat Transfer* (Edited by W. J. Minkowycz, E. M. Sparrow, G. E. Schneider and R. H. Pletcher), pp. 89–116. Wiley, New York (1988).
17. G. X. Wang and E. F. Matthys, Modelling of rapid solidification by melt-spinning: effect of heat transfer in the cooling substrate, *Mater. Sci. Engng* **A136,** 85–97 (1991).
18. Z. Gong, P. Wilde and E. F. Matthys, Numerical modelling of the planar flow melt-spinning process, and experimental investigation of its solidification puddle dynamics, *Int. J. Rapid Solidification* **6**(1), 1–28 (1991).
19. M. I. Eskenazi and E. F. Matthys, Modelling of planar flow melt-spinning using the boundary layer equations, Report No. UCSB-ME-88-4, University of California, Santa Barbara (1988).
20. K. H. Tacke, Discretization of the explicit enthalpy method for planar phase change, *Int. J. Numer. Meth. Engng* **21,** 543–554 (1985).
21. P. Wilde and E. F. Matthys, Experimental investigation of the planar flow casting process: development and free surface characteristics of the solidification puddle, *Mater. Sci. Engng*, in press.
22. H. A. Davies, Solidification mechanisms in amorphous and crystalline ribbon casting. In *Rapidly Quenched Metals* (Edited by S. Steeb and H. Warlimont), pp. 101–106. Elsevier Science, Amsterdam (1985).
23. E. M. Gutierrez, The mathematical modeling of rapid solidification processing, Ph.D. Thesis, Massachusetts Institute of Technology, Cambridge, Massachusetts (1985).
24. E. Vogt, On the heat transfer mechanism in the melt spinning process, *Int. J. Rapid Solidification* **3,** 131–146 (1987).
25. S. C. Huang and H. C. Fiedler, Effects of wheel surface conditions on the casting of amorphous metal ribbons, *Metall. Trans. A* **12A,** 1107–1112 (1981).
26. K. Takeshita and P. H. Shingu, Thermal contact during the cooling by the single roller chill block casting, *Trans. Japan Inst. Metals* **27,** 454–462 (1986).
27. G. X. Wang and E. F. Matthys, Modelling of heat transfer and solidification during splat cooling: effect of the splat thickness and splat/substrate thermal contact, *Int. J. Rapid Solidification* **6,** 141–174 (1991).
28. G. X. Wang and E. F. Matthys, Heat transfer modelling of rapid solidification on a substrate: a parametric investigation for large undercooling, *Int. J. Rapid Solidification*, in press.

MODELISATION NUMERIQUE DU CHANGEMENT DE PHASE ET DU TRANSFERT THERMIQUE PENDANT LA SOLIDIFICATION RAPIDE: UTILISATION DES INTEGRALES DE VOLUME DE CONTROLE AVEC SUBDIVISION ELEMENTAIRE

Résumé—Un schéma est développé pour la modélisation numérique du transfert thermique et du changement de phase pendant la solidification rapide. Cette technique est basée sur les intégrales de volume de contrôle et atteint une haute résolution pour l'interface solide–liquide par subdivision élémentaire. Elle convient particulièrement bien pour la solidification rapide avec sous-refroidissement, une prédiction précise de la température à l'interface pendant la recalescence étant très importante. Cette approche est utilisée pour la modélisation de la coulée continue planaire et la solidification en plaque. Quelques résultats sur les profils de température, sur la localisation et la vitesse de l'interface, le sous-refroidissement et le flux thermique sont montrés pour les deux mécanismes.

NUMERISCHE BESCHREIBUNG VON PHASENWECHSEL UND WÄRMEÜBERTRAGUNG WÄHREND EINES SCHNELLEN ERSTARRUNGSVORGANGS MIT HILFE VON KONTROLLVOLUM-INTEGRALEN UND AUFTEILUNG IN UNTERELEMENTE

Zusammenfassung—Zur numerischen Beschreibung des Phasenwechsels während eines schnellen Erstarrungsvorgangs wird ein effektives Verfahren für die Grenzflächenbewegung entwickelt, das auf Kontrollvolum-integralen beruht. Durch weitere Unterteilung der Kontrollelemente zur Beschreibung der Bewegung der Fest/Flüssigphasengrenze erhält man eine hohe Auflösung. Diese Methode bietet sich besonders bei der schnellen Erstarrung mit Unterkühlung an, für die eine genaue Vorhersage der Grenzflächentemperatur sehr wichtig ist. Das Verfahren wird zur Modellierung der Vorgänge beim ebenen Fließgießen und beim Spritzkühlen benutzt. Für beide Prozesse werden einige Ergebnisse vorgestellt: Temperaturprofile sowie Grenzflächengeschwindigkeiten, -verläufe, -unterkühlungen und Abkühlgeschwindigkeiten.

ЧИСЛЕННОЕ МОДЕЛИРОВАНИЕ ФАЗОВОГО ПЕРЕХОДА И ТЕПЛОПЕРЕНОСА В ПРОЦЕССЕ БЫСТРОГО ЗАТВЕРДЕВАНИЯ: ИСПОЛЬЗОВАНИЕ ИНТЕГРАЛОВ КОНТРОЛЬНЫХ ОБЪЕМОВ С ПОДРАЗДЕЛЕНИЕМ НА ЭЛЕМЕНТЫ

Аннотация—Разработана эффективная схема слежения за перемещением границы раздела, предназначенная для численного моделирования теплопереноса и фазового перехода в процессе быстрого затвердевания. Предложенный метод основан на интегралах контрольных объемов и обеспечивает прослеживание с высокой разрешающей способностью за перемещением границы раздела твердое тело/жидкость посредством подразделения контрольных объемов на отдельные элементы. Этот метод наиболее удобен для описания быстрого затвердевания в условиях недостаточного охлаждения, когда очень важным является точный расчет температуры на границе раздела при рекалесценции. Указанный подход использовался для моделирования процессов плоского литья и импактного охлаждения. Показаны некоторые результаты по температурным профилям, скорости и расположению границы раздела, а также степени и интенсивности охлаждения в обоих процессах.